Nuclear Materials Authority
P.O.Box 530 Maadi, Cairo, Egypt

ISSN 2314-5609
Nuclear Sciences Scientific Journal
9A, 43- 61
2020
http://www.ssnma.com

GEOCHEMISTRY OF THE MIOCENE SANDSTONE AND SHALE AT UM GREIFAT AREA, CENTRAL EASTERN DESERT, EGYPT: IMPLICATIONS TO PROVENANCE, TECTONIC SETTING AND RARE EARTH ELEMENTS POTENTIALITY

MOUSTAFA H. HASHAD; FAROUK M. SOLIMAN; GEHAD M. SALEH[1]; SAMEH H. NEGM[1]; MAHMOUD M. BADRAN[1] and TAREK F. MOHAMMADEN[1]
Faculty of Science, Suez Canal University ;[1] Nuclear Materials Authority, Cairo, Egypt

ABSTRACT

The studied Miocene sandstone and shale rocks are belonging to El-Ranga Formation. Petrographically, the sampled sandstone is classified as sublitharenite with evidence on variable transportation distances and derivation from sedimentary, igneous and/or metamorphic rocks. The iron oxides appear as the dominant cementation while quartz is the main matrix material in this sandstone. On the other hand, the shale appears as silty-to sandy shale consisting of fine to very fine, subangular to angular and moderate to poor sorted grains. Mutual bands of the black manganese oxides and brownish-yellow iron oxides are sometimes observed with indication of silica-rich solutions post-dated the formation of these bands.

Geochemically, the studied rocks were confirmed as sublitharenite and shale rich in iron. The active continental margin and island arc appeared the probable tectonic settings for Um-Greifat sandstone and shale, respectively. The quartzose sedimentary provenance and the mafic igneous provenance are expected as the primary provenances for the sandstone and shale respectively. The total REE content in the sandstone samples ranged between 0.49% and 0.83% while in the shale samples it ranged from 288 to 526 ppm and the accessory minerals are the main factor controlling the REE concentration and distribution particularly in Um-Greifat sandstone.

INTRODUCTION

To the south of Egypt, the Red Sea range abuts against the Red Sea Coast leaving a narrow maritime plain where pre-Miocene sediments (Cretaceous and Eocene) were eroded while in the Quseir-Safaga district, the strike faults gave rise to a remarkable topographical complexity in which the pre-Miocene strata are preserved (Said 1990). On the other hand, the Miocene and later sediments form a strip along the Red Sea Coast exhibiting marked lithological changes laterally and vertically and they rest unconformably with a depositional dip on older rocks.

Several geological classifications have been adopted to the stratigraphic succession along the Red Sea Coast (e.g. El-Akaad and Dardir, 1966; El Badry et al., 1986; Said, 1990; Hassan, 1990 and Abd El-Wahed et al., 2010). Accordingly, different formations were recognized such as; El-Ranga Formation, Um Mahara Formation, Abu Dabbab Forma-

tion, Um Gheig Formation, Samh Formation, Gabir Formation, the Shagra Formation and the Pleistocene reef. These formations were described by many workers (e.g. Philobbos & El-Haddad, 1983; Abu Khadrah & Wahab, 1984; Khedr, 1984 and Said, 1990) and their features could be briefed as follows:

El-Ranga Formation overlies unconformably the older sediments where its lowest bed is a polymictic conglomerate derived mainly from the basement with rounded to angular clastics and is embedded in a red-brown sandy matrix. This basal conglomerate is followed upward by long series of fine to medium-grained sandstones of varying colors and minor shale beds.

Um Mahara Formation overlies unconformably the Ranga Formation with separation by thin conglomerate bed although both of the formations were first described as one unit (Gabal El Rusas Formation) by El-Akkad and Dardier (1966). Um Mahara Formation is made up of massive sandy limestone and gypsifosrous limestone members with veritable coralline reefs (Samuel and Saleeb, 1977).

Abu Dabbab Formation consists of solid white gypsum with rare intercalated shale while the sands and gravel are practically absent. Dolomitic or semi-crystalline limestone of irregular hard and compact masses is the only common intercalation with Abu Dabbab gypsum. *Um Gheig Formation* overlies Abu Dabbab Formation with limited thickness. It is a grain-stone (mud-free carbonate rock) rich in algae and bioclastics and seems to have been deposited in agitated shallow water above the wave base.

Samh Formation overlies unconformably Abu Dabbab Formation or Um Gheig Formation and composed upward of green to grey shale, fine-grained variegated sandstone, hard sandstone and limestone with occasional conglomerate.

Gabir Formation overlies the Samh Formation with seeming conformity. It is mainly composed of sandstone (about 124 m. in thickness) and lesser thickness beds of marls, reefal limestone, calcareous grits and gravel to the upward direction.

The Shagra Formation is followed unconformable by a succession of arkosic sandstones and minor marls and it is assigned to the Pliocene with a thickness reaches to 22 m. *The Pleistocene reef* is a 34 m. thick section made up of four successive organic reefs separated by conglomerate and gravel beds.

The current work concerns with the Miocene sandstone and shale rock units which confined to El-Ranga Formation at Um-Greifat area along the Red Sea Coast at the Central Eastern Desert. Petrographic and geochemical characteristics of these rocks were the matter of this study to investigate their potentiality as promising sources for some strategic and economic rare metals.

GEOLOGIC SETTING

Um-Greifat area locates along the Red Sea coast between lat. 25° 30' and 25° 33' N and long. 34° 33' and 34° 35' E and boarded by G. Abu Dob from the west direction (Fig. 1)

The sedimentary sequence in Um-Greifat area ranges from Miocene rocks composed of sandstone and shale (Figs. 2 & 3) up to Pleistocene facies of sandstone and shale. This thick succession overlies unconformably the basement rocks including granites (Hassan et al., 1990). Alluvial fan of recent sands and gravels of considerable thickness occurs in close to the sedimentary hills in Um-Greifat (Fig. 4). These alluvial deposits originated from the disaggregation of the surrounding rocks.

Different mineralization lenses are observed in Um-Greifat sediments including hematite, limonite, manganese, zinc and lead oxides. Also, discontinuous, short and variable thickness gypsite layers are occasionally encountered into these sedimentary successions (Fig. 5). The observed wide dissemination of the mineralized lenses in Um-Greifat indicates occurring of different turbidity pro-

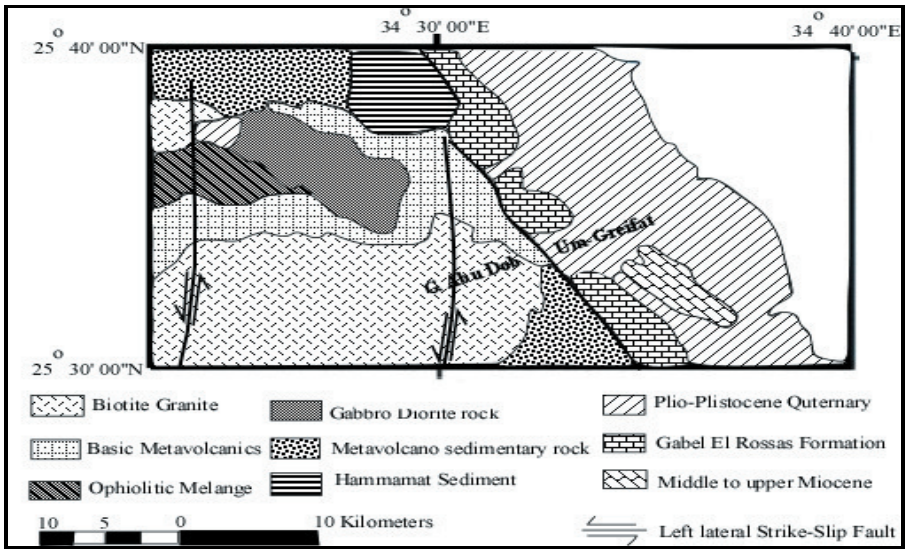

Fig. 1: Geological map of G. Um Greifat District, Central Eastern Desert, Egypt (After Ramadan et al., 1990)

Fig. 2: Photograph shows Gabal Um-Greifat sandstone

Fig. 3: Photograph shows Gabal Um-Greifat shale

cesses (Ammar, 1997).

The GIS investigation pointed to that the uranium mineralization is confined mainly to the NW-SE trending fault zone that cuts the Miocene clastic-carbonate sediments in Um-Greifat where the radioactive anomalies were recorded at several sites along the iron ochre mine which hosted in these sediments (Ramadan et al., 1990). In the same regard, Ammar (1997) ascribed the uranium mineralization-source to the hydrothermal solution associated with Tertiary volcanicity or due to the weathering products derived from the uraniferous granitic pluton. Also, Ammar (2007) pointed to presence of uranothorite mineral in association with jacobsite and other iron oxides (goethite and hematite) and suggested its derivation from the surrounding basement rock.

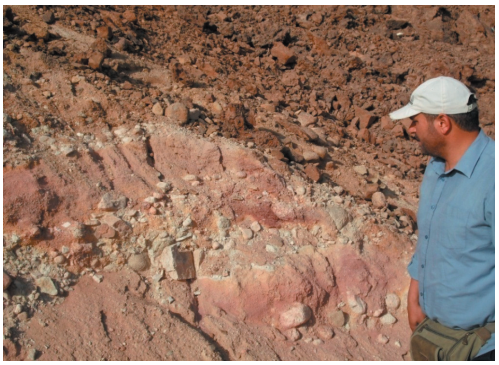

Fig. 4: Photograph shows Gabal Um-Greifat shale and alluvial deposits of sandstone and gravels

Fig. 5: Photograph shows discontinuous gypsum layers in G. Um-Greifat sandstone

METHDOLOGY

The petrographic characteristics of the studied rocks were obtained through the microscopic investigation of eight and seven thin sections of both Um-Greifat sandstone and shale respectively.

On the other hand, the major, trace and rare earth elements contents of these rocks were chemically analysed and determined. The major elements were analysed by the wet chemical techniques according to Shapiro and Brannock (1962). The trace elements were measured in the powdered form using the X-ray fluorescence (XRF) instrument under the conditions of W-target tube, LIF-220 crystal, gas flow proportional counter and scintillation counter 70 kv and 15 mA with detection limit 2 ppm. The rare earth elements (REE) were measured using the inductively coupled plasma-mass spectrometry (ICP-MS) which installed in the National Research Center, Cairo. The analytical precision for the measured elements was found as ± 2% for major elements and from ± 3% to 5% for both trace and rare earth elements.

For the major and rare earth elements, the investigated solid samples were firstly converted to the soluble phase where 10 grams of each sample (obtained by careful quartering of the original crushed sample) were ground to less than 0.063 mm (-200 mesh) in size. After the well homogenization, 0.5 gram was accurately weighted and subjected to either acid or alkaline attack (based on the kind of the required measured element) under aggressive heating conditions. Finally, the attacked samples were dissolved in de-ionized water and up to volume of 250 ml using the same water kind. On the other hand, 2 grams were weighted after the well quartering from the ground samples (-200 mesh size) and directly delivered to the XRF instrument for the trace elements determination.

PETROGRAPHICAL STUDIES

Sandstone

Petrographically, Um Greifat sandstone is likely to be classified as sublitharenite where the quartz grains constitute about 85% or more from the total mineral composition with rock fragments reach up to 10%. Absence of the clay matrix and the approximate nil of the feldspar components were clearly observed in the studied thin sections (Figs. 6, 7 & 10). Scarcity or absence of the feldspars is reasonably interpreted due to their easily weathering. The rock appears to be of mature stage where no clay matrix with well to moderate sorted grains of common low sphericity and

sub-rounded to sub-angular shape (Fig. 6)

The quartz grains are mostly found as monocrystalline showing no undulose extinction however, the polycrystalline grains were also observed exhibiting straight or sutured boundaries (Fig. 7) with the undulose extinction. The straight boundaries usually indicate the igneous rocks source of these grains while the sutured boundaries indicate derivation from a metamorphic source. Blatt (1992) believed that the undulatory quartz is more common in the coarse fraction of naturally disintegrated primary source rocks. The degree of grain-roundness, the presence of monocrystalline and polycrystalline grains as well as the straight and sutured boundaries reflect that the quartz grains were transported along variable distances and derived from various sources; sedimentary, igneous and metamorphic rocks.

In addition, the quartz grains sometimes show incorporation of small needle-shaped inclusions appear as dark specks which could be the fluids that present at the time of crystallization and known as fluid inclusions or vacuoles (Fig. 8). Such feature may indicate the derivation of the quartz grains from low-temperature origin such as the hydrothermal veins. Occasionally, the grain contacts are not common (Fig. 9) giving the floating grains fabric which might be evidence of an early stage of cementation (Bishay, 1994).

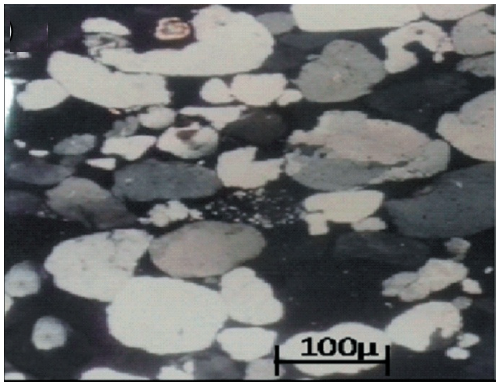

Fig. 7: Photomicrograph shows polycrstalline qz-grains with sutured boundaries, calcite cement (at the photo center) as well as grains with authigenic Qz-cementation (bottom corner at the left-hand side)

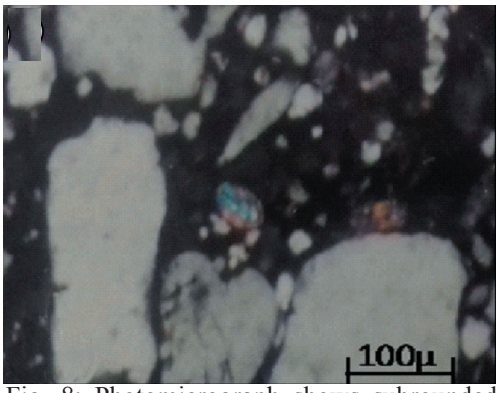

Fig. 8: Photomicrograph shows subrounded quartz grains, elliptical zircon and matrix composed maily of small Qz-grains. Dark specks incluions are observed in the large Qz-grain at the photo base

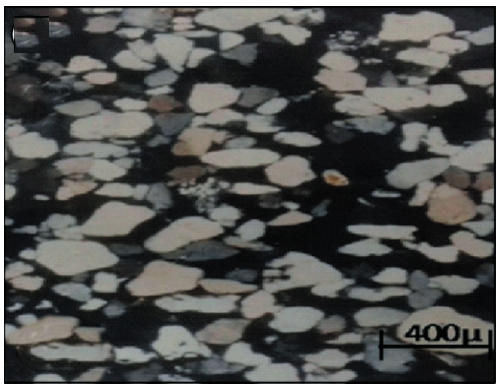

Fig. 6: Photomicrograph shows low sphericity, subrounded to subangular well sorted quartz grains with iron oxide cementation

The matrix materials are only represented by quartz grains (Figs. 8 & 11). On opposite, different cementation types were observed in the studied sandstone represented in quartz, calcite and iron oxides cement materials. The

Fig. 9: Photomicrograph shows floating-granis fabric and relics of bended mica, all in iron oxides cementation

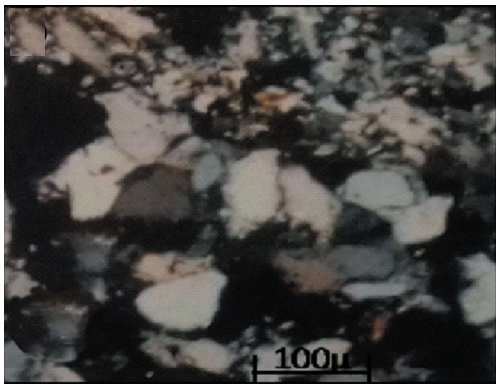

Fig. 10: Photomicrograph shows subangular quartz grains, quartz overgrowth, iron-coated elliptical zircon and rock fragment probably of sandstone type

secondary (authigenic) quartz sometimes appeared as poorly-developed overgrowth cementation; also the calcite is occasionally formed the cement material between the detrital quartz grains (Fig. 7). However, the iron oxides appear as the most dominant cementation replacing the majority of other cement types. At these localities, the ferruginous sandstone becomes hematitic sandstone to sandy hematite with subangular to subrounded, medium to fine randomly oriented quartz grains showing variable degrees of packing.

Mica of bended flakes was recorded as a part of rock fragment component (Fig. 9). The accessory minerals were observed, mainly represented by zircon and fluorite, but sometimes they don't appear due to their coating by or embedding into the cementation materials particularly the iron oxides (Figs. 8 & 10).

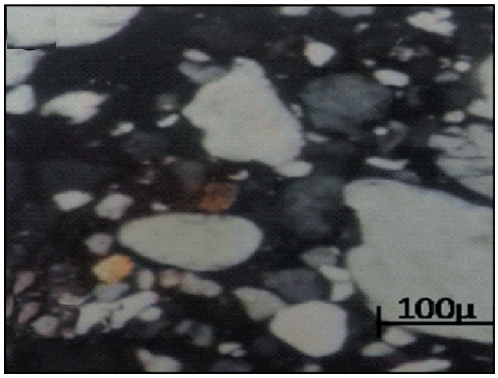

Fig. 11: Photomicrograph shows subrounded quartz grains of moderate sorting and the matrix mainly composed of small quartz grains of different orientations

Shale

Under the microscope, it appears as silty- to sandy-shale consists of fine to very fine, angular to subangular and moderate to poor sorted quartz grains that are embedded in clay matrix (Fig. 12). Green copper grains could be indentified with the iron oxides as fissure filling.

Mutual bands of the black manganese oxides and brownish-yellow iron oxides were observed and usually accompanied by fine angular to subangular quartz grains which may indicate silica-rich solutions postdated the formation of these manganese and iron bands (Fig. 13).

GEOCHEMICAL CHARACTERISTICS

To configure the chemical composition and the geochemical characteristics of Um

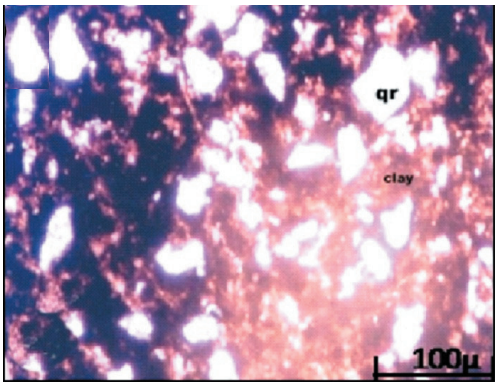

Fig. 12: Photomicrograph shows sandy-shale composed of moderate sorted, angular to subangular fine quartz grains embdded in the clay matrix

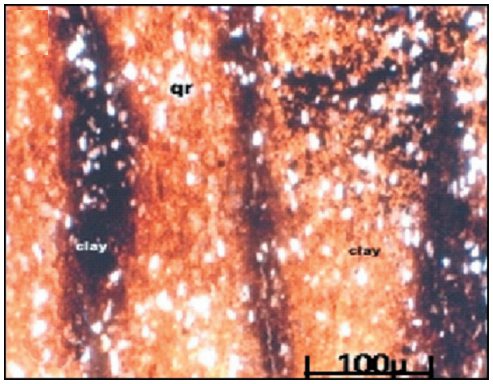

Fig. 13: Photomicrograph shows mutual bands of black Mn-oxides and brownish-yellow Fe-oxides with postdate silica activity

Greifat sandstone and shale rocks, eight samples of each were subjected to the chemical analysis for their major and trace components (Tables 1 & 2), while only 5 samples of each rock were selected for the REE determination (Table 3).

Bivariant Relationships

The bivariant diagrams of SiO_2 versus the other major oxides and trace elements of Um-Greifat sandstone and shale showed the samples scattering as the common trend relative to linear and curvilinear trends (Figs. 14-33). In the clastic sedimentary rocks; the scattered trends result from three-component mixing (quartz-illite-calcite) with taking in account as the SiO_2 increases as the mineralogical maturity increases (i.e. a greater quartz content and smaller proportion of other detrital grains) Argest and Donnelly (1987).

Chemical Classification

The binary diagram of log (SiO_2/Al_2O_3) versus log ($Fe_2O_3^t/K_2O$) according to Herron (1988) is used for the classification of the terrigenous sandstones and shales. Plotting of the investigated samples revealed the sandstone more relates to the sublitharenite rich in iron and also the studied shale was assigned as Fe-shale (Fig. 34). The sandstone classification was confirmed using the bivariance diagram [log (Na_2O/K_2O) versus log (SiO_2/Al_2O_3)] after Pettijohn et al. (1972) and modified by Herron (1988), where the tested sandstone samples emphasized their sublitharenite type (Fig. 35).

The Multi-element Diagrams

The processes controlling the trace elements composition of sedimentary rocks may be investigated using the normalization diagrams although they are not as widely used as their equivalents in the igneous rocks.

Um-Gerifat sandstone samples were normalized relative to the values of the average Phanerozoic quartz arenite which given by Boryta and Condie (1990) while the shale samples were normalized relative to the values of the North American Shale Composite (NASC) which given by Gromet et al. (1984). The resultant spider diagrams (Figs. 36 and 37) showed that the sandstone has obvious positive Fe anomaly which is likely ascribed to the effect of the Fe-rich solutions which invaded the sandstone after its deposition while the role of the ferromagnesian minerals could be ignored particularly with the depletion of Ti and Cr elements as well as the scarcity of these minerals as shown from the mineral-

Table 1: Major elements concentrations (wt %) of Um-Greifat sandstone and shale

	S.NO.	SiO_2	TiO_2	Al_2O_3	Fe_2O_3t	MgO	CaO	Na_2O	K_2O	P_2O_5	LOI	Total
Sandstone	1	84.31	0.08	0.78	12.3	0.08	0.12	0.78	0.10	0.08	2.31	100.8
	2	85.16	0.02	0.78	10.1	0.05	0.14	0.78	0.21	0.09	2.60	99.90
	3	86.13	0.07	1.13	10.3	0.04	0.14	1.10	0.17	0.02	2.22	101.4
	4	85.22	0.03	1.35	12.3	0.02	0.15	0.43	0.23	0.02	1.61	101.3
	5	81.17	0.05	1.12	15.7	0.06	0.14	1.10	0.17	0.08	1.66	101.2
	6	81.12	0.02	0.73	15.2	0.06	0.11	0.73	0.12	0.01	2.11	100.3
	7	85.92	0.04	1.26	9.30	0.04	0.11	1.26	0.24	0.02	2.61	100.8
	8	82.88	0.09	1.54	14.1	0.06	0.11	0.54	0.19	0.03	2.11	101.7
	AV.	83.98	0.05	1.08	12.4	0.05	0.12	0.85	0.17	0.04	2.15	
Shale	1	22.5	0.13	20.1	24.4	3.63	12.1	1.25	0.10	0.09	15.7	100.1
	2	18.4	0.15	20.4	21.2	4.13	16.3	2.70	1.01	0.12	15.2	99.61
	3	19.5	0.17	15.1	17.6	6.80	18.4	2.40	0.40	0.21	18.9	99.48
	4	23.1	0.12	17.2	22.4	5.60	17.5	0.78	1.05	0.12	13.1	101.0
	5	23.4	0.12	18.8	24.3	5.90	14.1	0.73	1.10	0.21	11.2	99.90
	6	21.3	0.13	19.3	16.1	6.10	19.1	1.54	0.1	0.09	18.1	101.9
	7	22.1	0.18	15.8	22.9	5.60	14.0	2.10	0.49	0.57	16.7	100.4
	8	19.1	0.10	16.1	26.1	7.30	16.8	1.10	1.20	0.51	12.3	100.6
	AV.	21.2	0.14	17.9	21.88	5.63	16.1	1.58	0.68	0.24	1.2	

Fe_2O_3t : Total iron as Fe_2O_3

Table 2: Trace elements concentrations (ppm) of Um-Greifat sandstone and shale

	S.NO.	Cr	Ni	Cu	Zn	Zr	Rb	Y	Ba	Pb	Sr	Ga	V	Nb
Sandstone	1	14	9	11	1531	179	16	19	325	138	202	6	18	12
	2	25	12	7	1357	251	8	12	165	74	115	5	37	8
	3	40	17	6	2324	116	7	8	211	81	315	3	17	4
	4	31	20	5	3312	79	5	13	215	124	225	4	23	8
	5	39	30	8	2156	88	11	5	131	153	216	3	24	5
	6	25	24	7	1659	121	3	8	221	110	125	2	11	2
	7	24	5	8	3113	135	17	7	179	97	219	8	9	11
	8	32	8	4	2516	98	6	9	181	78	213	2	19	7
	AV.	29	16	8	2246	133	9	10	206	107	204	4	20	7
Shale	1	46	31	10	8684	257	18	23	53	131	55	4	67	14
	2	32	55	13	9140	145	21	21	53	56	44	7	70	12
	3	28	23	5	> 10000	135	3	12	75	75	28	3	84	5
	4	51	25	7	7278	104	19	11	70	52	15	2	121	5
	5	87	12	3	9643	140	7	18	44	78	33	14	59	9
	6	62	19	10	8303	100	9	10	30	81	14	2	59	5
	7	45	84	13	> 10000	173	5	7	26	72	16	9	73	4
	8	61	70	10	> 10000	71	14	7	54	57	19	5	102	4
	AV.	51.5	39.9	8.9	8610	140.6	12.0	13.6	50.6	75.3	28.0	5.8	79.4	7.3

ogical study. Also, the positive Sr anomaly suggests a mitigated effect of the weathering processes on the sandstone (Wronkiewicz and Condie, 1987). Depletion of Zr usually points to the low zircon-contents in the investigated rocks hence its limited effect on abundance and distribution of the zirconium element in Um-Greifat sandstone.

On the other hand, the spider diagram of shale showed depletion in most of elements except the +ve anomalies of both Ca and Fe. Such phenomenon may point to the wide weathering effect which caused the leachability of many elements while the Ca and Fe ele-

Table 3: The REE contents (ppm) in Um-Greifat sandstone and shale rocks

	S.NO.	La	Ce	Pr	Nd	Sm	Eu	Gd	Tb	Dy	Ho	Er	Tm	Yb	Lu
Sandstone	1	97	127	23	114	165	9	715	265	1915	518	1715	325	1880	263
	2	104	141	45	192	102	8	850	254	2304	581	1873	221	1411	199
	3	84	187	34	123	119	6	358	511	901	418	1167	335	944	313
	6	131	183	41	139	129	7	663	212	997	422	1272	236	1141	214
	7	125	109	18	164	128	6	322	313	830	426	917	253	913	402
	AV.	108	149	32	146	129	7	582	311	1389	473	1389	274	1258	278
Shale	1	79	137	13	59	11	2	8	12	7	12	4	6	14	11
	2	118	191	21	108	21	3	11	8	9	10	7	5	17	11
	3	137	232	26	131	25	4	12	6	7	11	8	3	16	12
	4	102	173	28	168	50	2	9	11	6	9	7	4	15	13
	5	77	300	22	116	44	5	11	9	8	11	6	5	18	10
	AV.	103	207	22	116	30.2	3.2	10.2	9.2	7.4	10.6	6.4	4.6	16	11.4

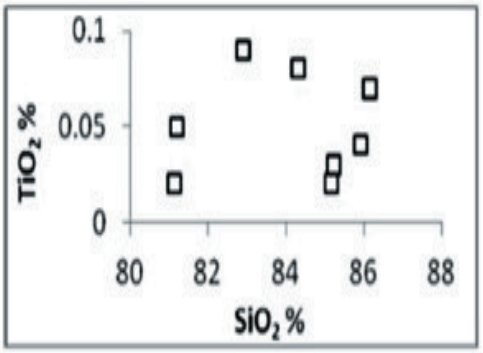

Fig. 14: SiO_2-TiO_2 diagram of the studied sandstone

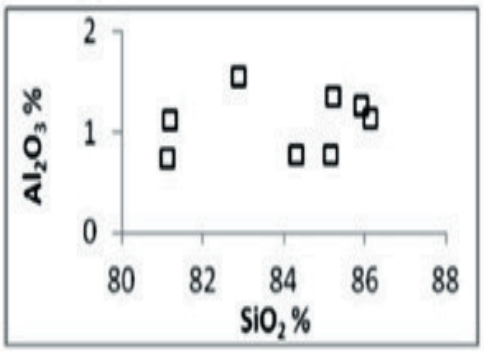

Fig. 16: SiO_2-Al_2O_3 diagram of the studied sandstone

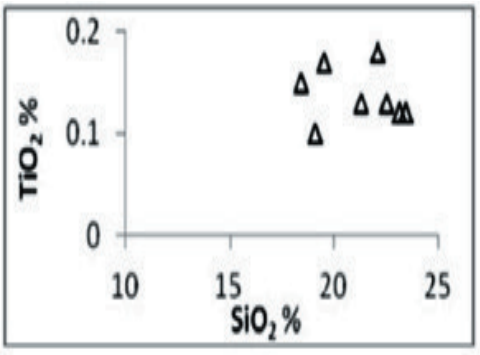

Fig. 15: SiO_2-TiO_2 diagram of the studied shale

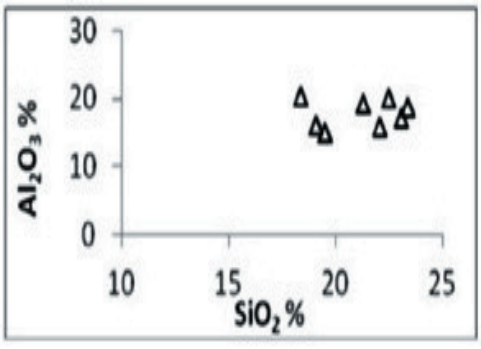

Fig. 17: SiO_2-Al_2O_3 diagram of the studied shale

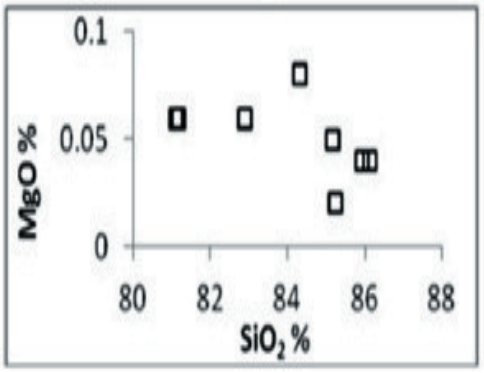

Fig. 18: SiO_2-MgO diagram of the studied sandstone

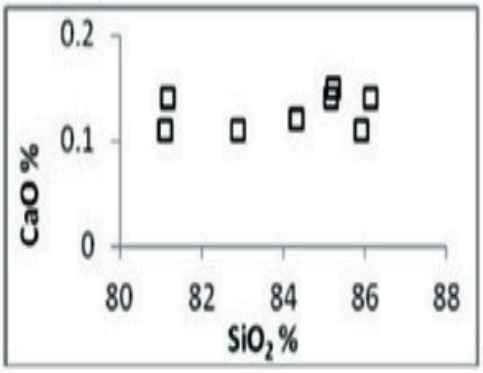

Fig. 21: SiO_2-CaO diagram of the studied shale

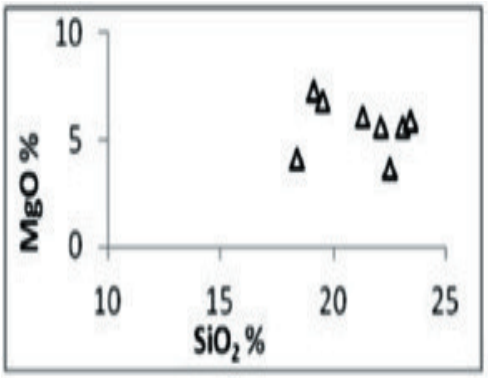

Fig. 19: SiO_2-MgO diagram of the studied shale

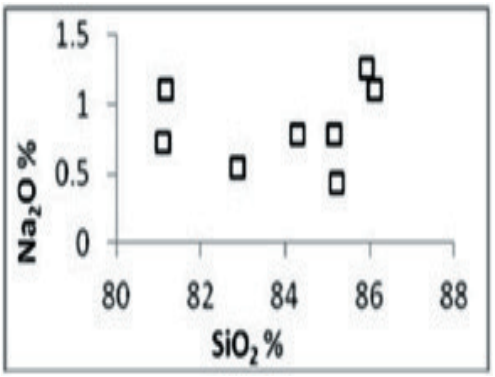

Fig. 22: SiO_2-Na_2O diagram of the studied sandstone

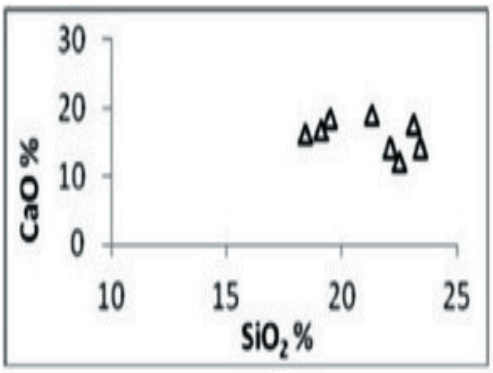

Fig. 20: SiO_2-CaO diagram of the studied sandstone

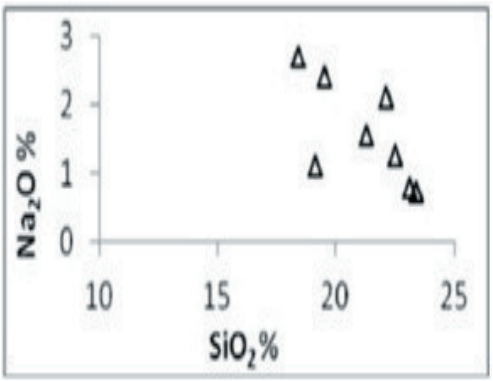

Fig. 23: SiO_2-Na_2O diagram of the studied shale

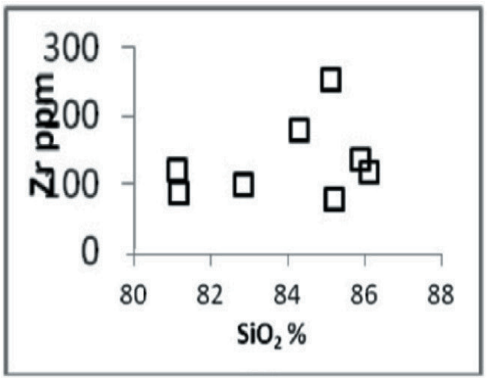

Fig. 24: SiO_2-Zr diagram of the studied sandstone

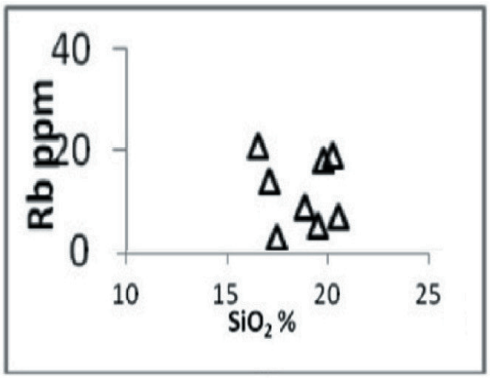

Fig. 27: SiO_2-Rb diagram of the studied shale

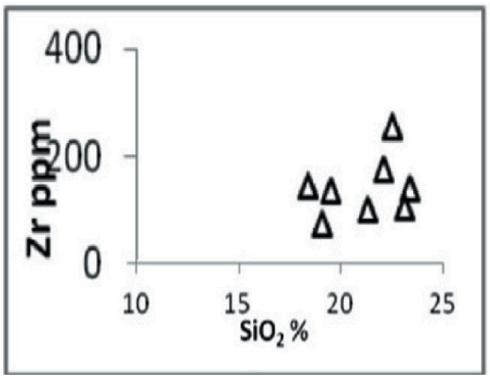

Fig. 25: SiO_2-Zr diagram of the studied shale

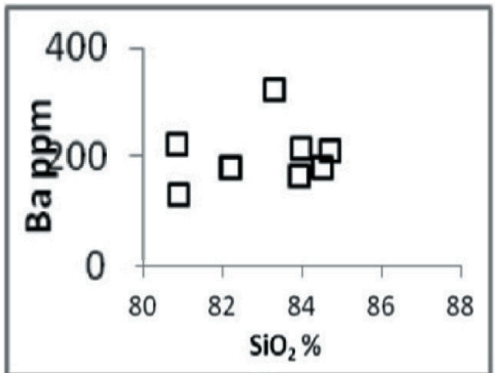

Fig. 28: SiO_2-Ba diagram of the studied sandstone

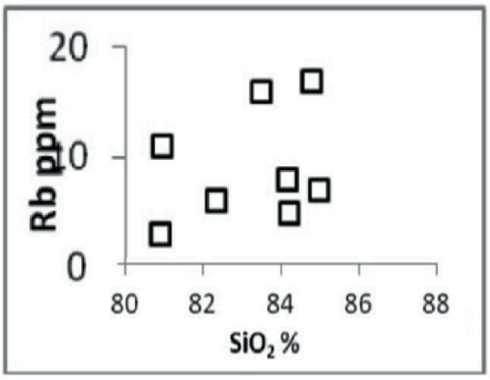

Fig. 26: SiO_2-Rb diagram of the studied sandstone

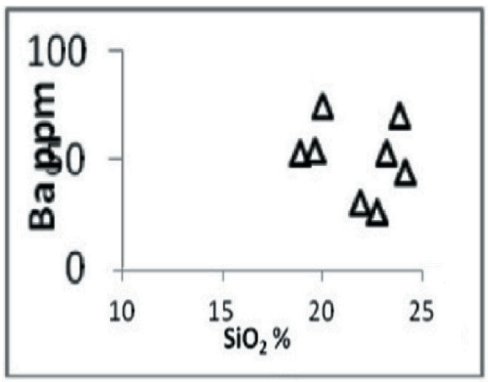

Fig. 29: SiO_2-Ba diagram of the studied shale

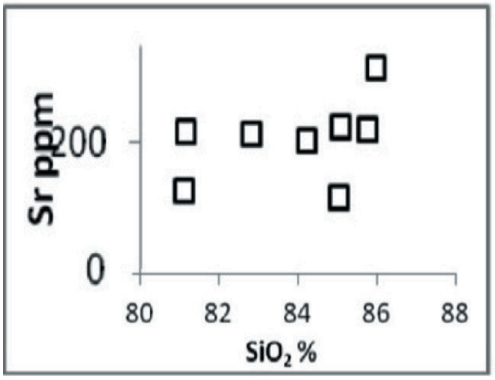

Fig.30: SiO_2-Sr diagram of the studied sandstone

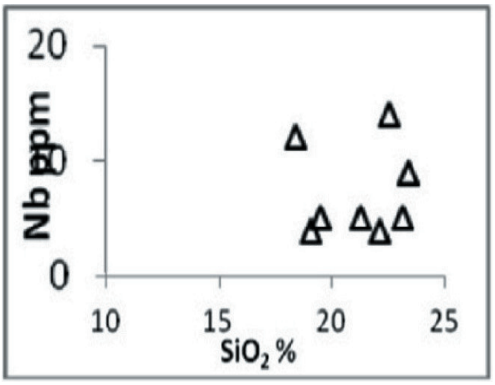

Fig.33: SiO_2-Nb diagram of the studied shale

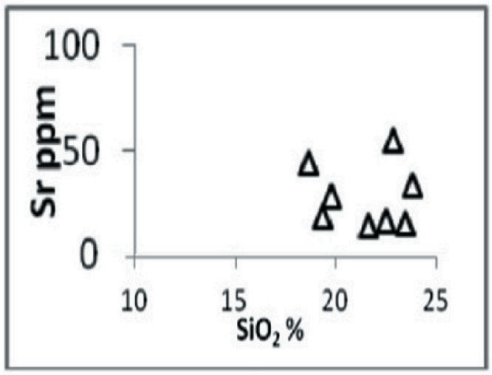

Fig.31: SiO_2-Sr diagram of the studied shale

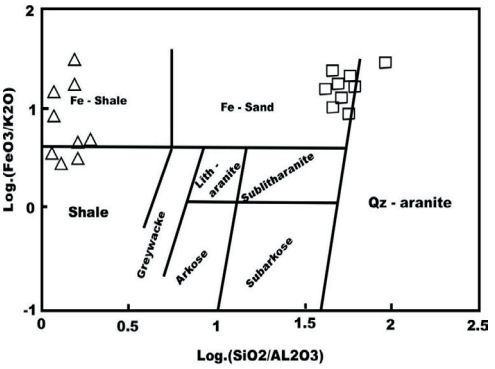

Fig. 34: Bivariance classification diagram after Herron (1988), (□) sandstone and (Δ) shale

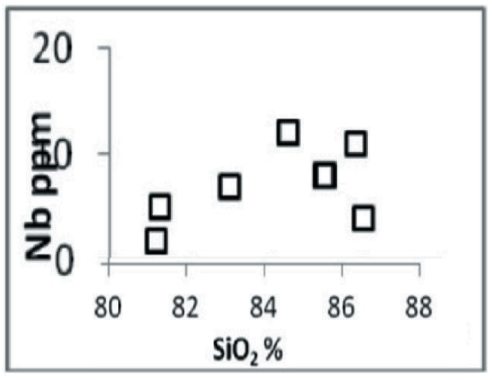

Fig.32: SiO_2-Nb diagram of the studied sandstone

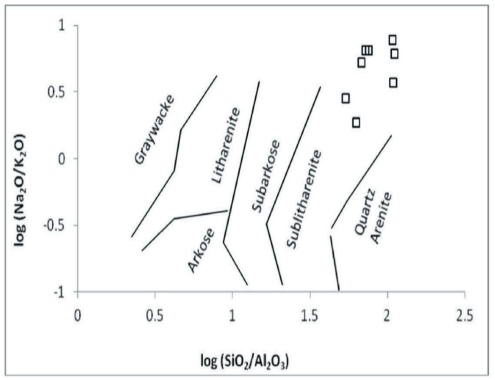

Fig. 35: Bivariance classification diagram after Pettijohn et al. (1972) modified by Herron (1988), for the studied sandstone

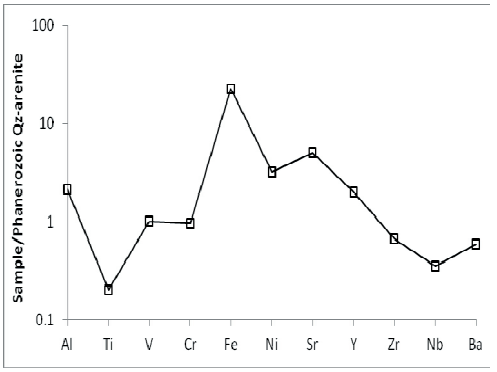

Fig. 36: The multi-elements spider diagram of Um-Greifat sandstone after normalization to the Phanerozoic quartz arenite (Boryta and Condie, 1990)

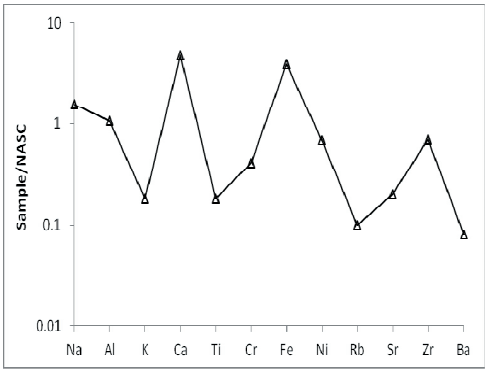

Fig. 37: The multi-elements spider diagram of Um-Greifat shale after normalization to NASC values (Gromet et al., 1984)

ments are mainly controlled by the Fe-bearing solution and the intercalated gypsum mineralization as revealed from the field work.

Tectonic Setting

The plate tectonic processes impart a distinctive geochemical signature to sediments (Bhatia and Crook, 1986).

Based on variability in the chemical composition of the modern clastic sediments from the oceanic and continental arcs and the passive and active continental margins, Roser and Korsch (1986) discriminate three tectonic settings using the K_2O/Na_2O versus SiO_2 and they tested the validity of this diagram using sand-mud modern sediments which plotted where expected.

Plotting of the relevant data of the studied samples on this diagram illustrated that the sandstone located around the active continental margin-passive margin boarder line with more tendency toward the active continental margin field. On the other hand, the shale samples showed the island arc as their probable tectonic setting (Fig. 38).

Provenance Signature Using the Major Elements

The discrimination binary diagram plotted as function of the major oxides (Roser and Korsch 1988) is used to discriminate the primary provenance of the sedimentary rocks. Plotting of the studied samples on this diagram revealed the quartzose sedimentary provenance as the primary provenance of the sandstone while the mafic igneous provenance appears the most probable primary provenance for Um-Greifat shale (Fig. 39). However, scarcity of the alkali feldspars in the studied rocks as well as the very low K_2O content is reasonably supporting the resulted provenance.

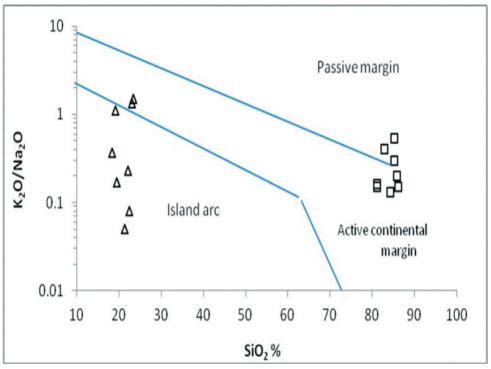

Fig. 38: SiO_2-K_2O/Na_2O tectono-discrimenation diagram after Roser and Korsch (1986), (Symbols as in Fig.34)

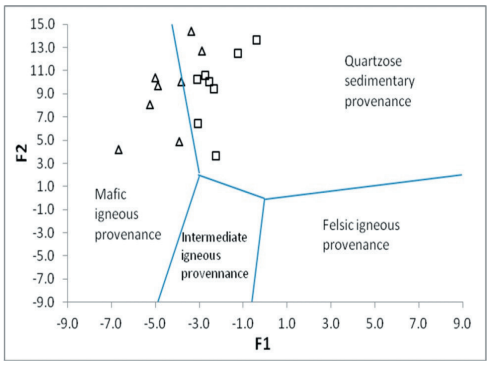

Fig. 39: F1 vs. F2 provenance-discrimenation diagram after Roser and Korsch (1988). (Symbols as in Fig.34)

Rare earth elements

The most important factor contributing to the REE content of clastic sediments is its provenance (McLennan, 1989). This is because the REE are insoluble and are chiefly transported as particulate matter and reflect the chemistry of their source, thus diagenitic processes have little influence on the redistribution of the REE. Also, the accessory and heavy minerals are important source of the REE in the sedimentary rocks particularly zircon, xenotime, monazite, allanite, garnet, apatite and sphene.

Five sandstone and five shale samples were analyzed using the ICP-MS for REE quantitative determination (Table 3). The total LREE (La, Ce, Pr and Nd), MREE (Sm, Eu, Gd, Tb, Dy and Ho) and HREE (Er, Tm, Yb and Lu) are given in Table (4).

The obvious and excited observation is the high REE concentration in the sandstone where it ranges from 0.49% to 0.83% represented mainly by the HREE then the MREE. On the other hand, the shale samples showed total REE ranges from 288 to 526 ppm in which the LREE represent 80% in average. These ratios should be dragged the attention for Um-Greifat sandstone as probable source for the REE exploitation.

REE-normalization

The REE data of the sandstone samples were normalized against the composition of the of the Upper Continental Crust (Taylor and McLennan, 1981) while the REE values of the studied shale samples were normalized against the North American Shale Composite, NASC (Gromet et al., 1984) and the averages of the normalized values were drawn (Figs. 40 & 41). The normalized diagrams showed high fractionation and medium fractionation in the sandstone and shale samples respectively with very high enrichment of both MREE and HREE relative to the LREE in the sandstone.

Table 4: Values of the total REE and their subgroups in the studied sandstone and shale

	S.NO.	TOTAL-REE	LREE	MREE	HREE	LREE/HREE
Sandstone	1	4926	361	3587	4183	0.09
	2	8131	482	4099	3704	0.13
	3	5500	428	2313	2759	0.16
	6	5787	494	2430	2863	0.17
	7	8285	416	2025	2485	0.17
	AV.	6525	435	2891	3199	0.14
Shale	1	375	288	52	35	8.23
	2	540	438	62	40	10.95
	3	630	526	65	39	13.49
	4	597	471	87	39	12.08
	5	642	515	88	39	13.21
	AV.	557	448	70.8	38.4	11.67

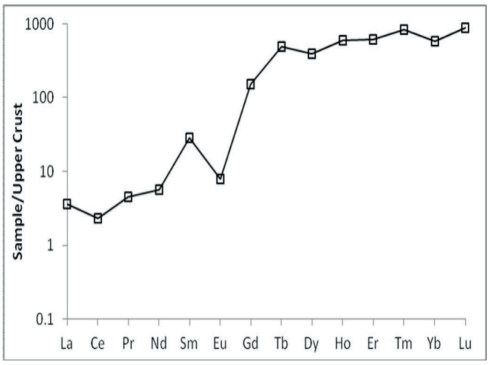

Fig. 40: The normalized REE pattern of Um-Greifat sandstone, the normalization is realtive to the upper crust values after Taylor and McLennan (1981)

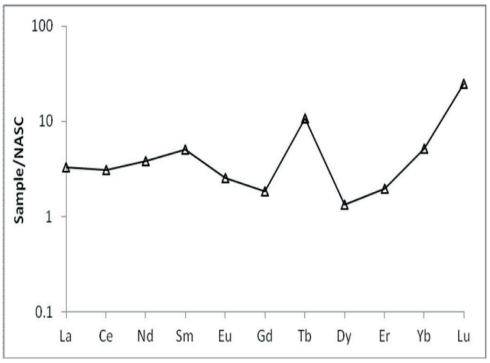

Fig. 41: The normalized REE pattern of Um-Greifat shale, the normalization is realtive to the NASC values after Gromet et al. (1984)

REE and the accessory minerals

Based on the obtained REE concentrations and the traditional role of some minerals in concentrate and control the distribution of the REE, it was necessary to investigate the effect of the recorded accessory minerals. Accordingly, the binary relations between the total REE for each analyzed sample and the corresponding values of P_2O_5, Zr, Y and Nb (as indicators for the monazite, zircon, allanite and samarskite minerals respectively) were plotted. The bivariance diagrams (Figs. 42 to 49) and the correlation values pointed to the following:

-Zircon, monazite and allanite minerals appear as the main controllers of the REE concentration and distribution in the sandstone.

-Referring to the partition coefficients of these minerals toward the REE, it is likely to propose that the zircon plays the major role in the HREE enrichment while the allanite and, in lesser order, monazite are responsible for the MREE concentrations.

-In the shale samples, the monazite mineral seems the only effective factor on the present REE concentration while the other accessory minerals have no importance in this regard. Such conclusion is supported by the more LREE abundance than the MREE and HREE in the shale samples where monazite has the highest partition coefficient toward the LREE among the other minerals.

CONCLUSIONS

From the aforementioned data of the petrographic and geochemical characteristics of Um-Greifat sandstone and shale rock units, some conclusions can be summarized as;

-Um-Greifat sandstone is originated from variable sources (igneous, metamorphic and sedimentary rocks) and slightly affected by the weathering processes. On the other hand, the hydrothermal solutions and the weathering processes practised a wide role on the shale rock unit.

-Both the rocks, particularly shale, are considered as Zn-bearing ore.

-The accessory minerals are the main factor controlling the REEs concentration and distribution particularly in Um-Greifat sandstone.

-Further studies shall be delivered to the Um-Greifat sandstone regarding the REE exploitation where the obtained data predict promising concentrations of these strategic

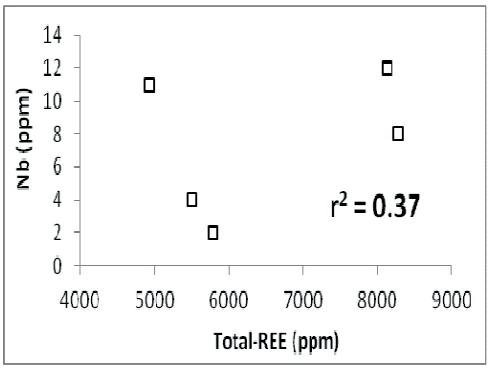

Fig.42: Total REE-Nb diagram of the studied sandstone

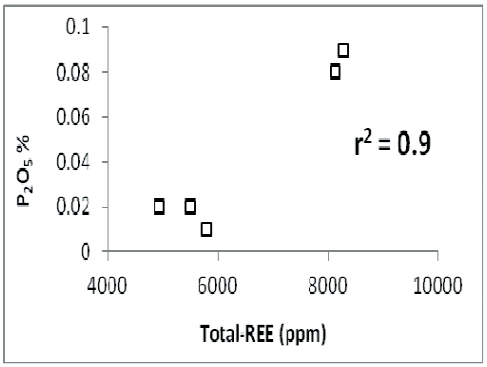

Fig.45: Total REE-P_2O_5 diagram of the studied sandstone

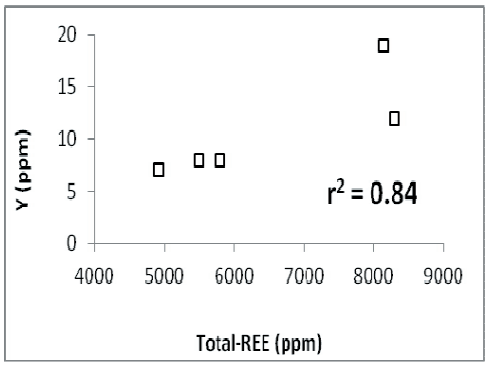

Fig.43: Total REE-Y diagram of the studied sandstone

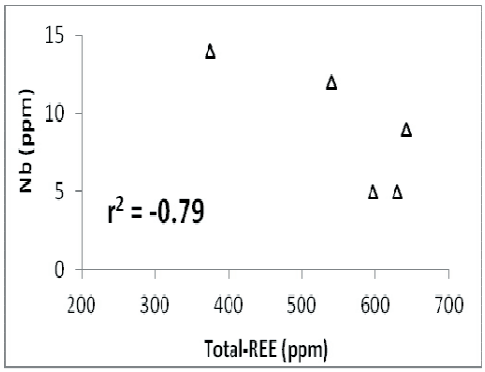

Fig.46: Total REE-Nb diagram of the studied shale

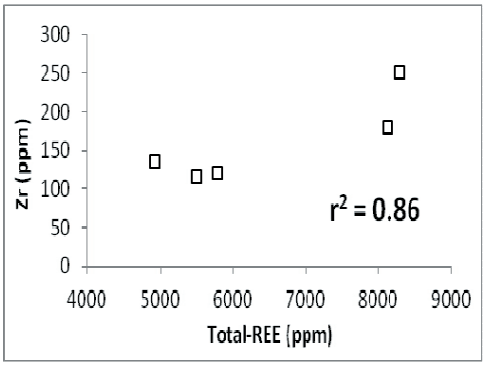

Fig.44: Total REE-Zr diagram of the studied sandstone

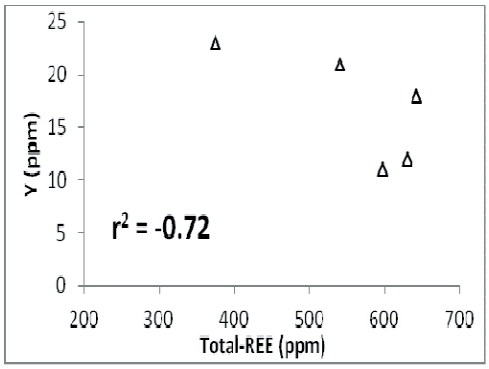

Fig.47: Total REE-Y diagram of the studied shale

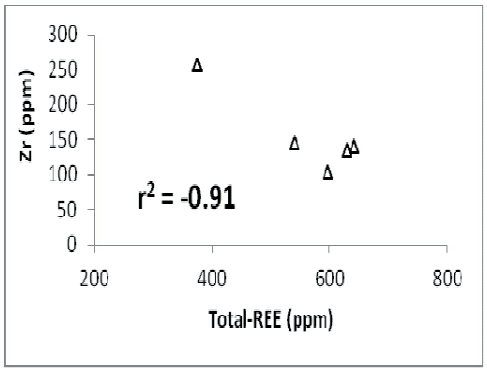

Fig.48: Total REE-Zr diagram of the studied shale

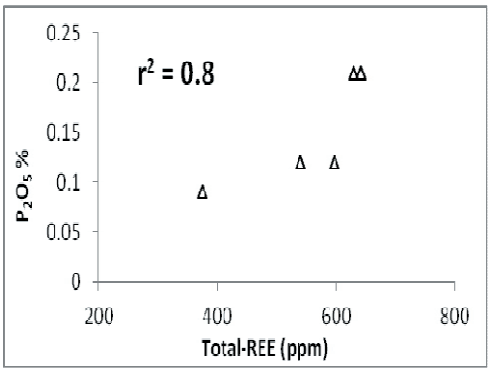

Fig.49: Total REE- P_2O_5 diagram of the studied shale

elements. In similar issue, Um-Greifat shale has to be considered as good source for economic recovery of Zn-metal.

REFERENCES

Abd El-Wahed, M.A.; Ashmawy, M.H., and Tewfik, H.A. 2010. Structural setting of Cretaceous pull-apart basins and Miocene extensional folds in Quseir–Umm Gheig region, northwestern Red Sea, Egypt. Lithosphere, 2, 13-32.

Abu Khadrah, and Wahab, S.A., 1984. Petrography and diagenesis of the Samh Formation and younger Sediments, north Marsa Alam area, Red Sea Coast, Egypt. J. Afr. Earth Sci., 2, 277-286.

Ammar, F.A., 2007. Mineralogical and Radiometric Studies for ochre-bearing Miocene Sediments, Um Greifat Area, Central Eastern Desert, Egypt. Sci. J. Fac. Sci., Menoufia Univ., XXI, 61-82.

Ammar, S.E., 1997. Uranium and thorium mineralization at northern part of Gabal Um Naggat Stock, Central Eastern Desert, Egypt. Sci. J., Mansoura Univ., 4, 12-46.

Argest, S., and Donnelly, T.W. 1987. The chemical discrimination of clastic sedimentary components. J. Sed. Petrol, 57, 813-823.

Bhatia, M.R., and Crook, K.A.W., 1986. Rare earth elements geochemistry of Australian Paleozoic greywacke and mud rocks: Provenance and tectonic control. Sedimentary Geol., 45, 97-113.

Bishay, A.F., 1994. Geological investigation and physical benefication of xenotime sediments of Um Bogma area, Sinai, Egypt. M.Sc. Thesis, Fac. Sci., Cairo Univ., Egypt, 188p.

Blatt, H., 1992. Sedimentary petrology. 2nd Ed., W.H. Freeman and company New York, 515p.

Boryta, M., and Condie, K.C., 1990. Geochemistry and origin of the Arcaean Beit Bridge complex, Limpopo Belt, South Africa. J. Geol. Sec. London, 147, 229-239.

El-Akkad, S., and Dardier, A. 1966. Geology of the Red Sea Coast between Ras Shagra and Mersa Alam with short note on results of exploratory work at Gabal El Russas lead-zinc deposits. Egypt. Geol. Surv., 35, 67-83.

El-Badry, O.A.; Hassaan, M.M.; Fathi, A.; El Khadragi, A., and Moursi, M., 1986. Contribution to lithostratigraphy and petrology of Middle Miocene rocks between Abu Shour and Ras Banas, Red Sea Coast, Egypt. Phaner. Devel. Egypt, 3rd Syrup., Cairo, Egypt, 10p.

Gromet, L.P.; Dymek R.F.; Haskin, L.A., and Korotev, R.L., 1984. The Northern American Shale Composite: Its compilation, major and trace element characteristics. Geochim. Cosmochim. Acta, 48, 2469-2482.

Hassan, M.M., 1990. Studies on lead–zinc sulphide Mineralization Red Sea Coastal Zone, Egypt. Proc., 8th IAGOD Symp. Ottawa, Canada, 835-847.

Herron, M.M., 1988. Geochemical classification of ferruginous sands and shale from core or leg data. J. Sed. Petrol., 58, 820-829.

Khedr, E., 1984. Sedimentological evaluation of the Red Sea continental margin of Egypt and its relationship to sea level changes. Sed. Geol., 39, 71-86.

McLennan, S.M., 1989. Rare earth elements in sedimentary rocks: Influence of the provenance and sedimentary process. In: Geochemistry and Mineralogy of Rare Earth Elements, 21, 169-200

Pettijohn, F.J.; Potter, P.E., and Siever, R., 1972. Sand and Sandstones. New York Springer-Verlag, 158p.

Philobbos, E.R., and El-Haddad, A.A., 1983. Contribution to Miocene and Pliocene lithostratigraphy of the Red Sea Coastal zone. 21st Ann. meeting, Geol. Soc. Egypt.

Ramadan, T.M.; El Mongy, S.A., and Salah El Dein, S., 1990. Exploration for Uranium and thorium mineralization at Wadi Um Laseifa area, Central Eastern Desert of Egypt: Using remote sensing technique. Australian. J. Basic and Applied Sciences, 689-697.

Roser, B.P., and Korsch, R.J., 1986. Determination of tectonic setting of sandstone-mudstone suites using SiO_2 content and K_2O/Na_2O ratio. J. Geol., 94, 635-650.

Said, R., 1990. The Geology of Egypt. Balkema, The Netherlands, 451-486.

Samuel, M.D., and Saleeb, R.G.S., 1977. Lithostratigraphy and petrography analysis of the Neogene sediments at Abu Ghusun, Um Mahara area, Red Sea Coast, Egypt. Beitr. Zur Lithologie, Freiburg Forsch., 323, 47-56.

Shapiro, L., and Brannock, W.W., 1962. Rapid analysis of silicate, carbonate and phosphate rocks. U.S. Geol. Surv. Bull. 1144A, 56p.

Taylor, S.R., and McLennan, S.M., 1981. The composition and evolution of the continental crust: Rare earth element evidence from sedimentary rocks. Phill. Trans. R. Soc. London, 301, 381-399.

Wronkiewicz, D.J., and Condie, K.C., 1987. Geochemistry of Archaean shales from the Witwatersrand Super group, South Africa: Sour cearea weathering and provenance. Geochim. Cosmochim. Acta, 51, 2401-2416.

جيوكيميائية صخرى الحجر الرملى والطفلة من عصر الميوسين بمنطقة أم جريفات، وسط الصحراء الشرقية، مصر: تطبيقات على نشأة التكوين والوضع التكتونى وإحتمالات العناصر الأرضية النادرة

مصطفى حسانين حشاد، فاروق محمد سليمان، جهاد محمد صالح، سامح حمدى نجم، محمود محمد بدران وطارق فهمى محمدين

تقع منطقة أم جريفات على ساحل البحر الأحمر بين خطى عرض٣٠ ' ٢٥ ° و٣٣'٢٥° شمالاً وخطى طول ٣٣'٣٤° و ٣٥'٣٤° شرقاً ويتكون التتابع الرسوبى من صخور الحجر الرملى والطفلة من عمر الميوسين إلى سحنات الحجر الرملى والطفلة من عمر البليستوسين.

وقد أشارت الدراسة البتروجرافية إلى أن الحجر الرملى من نوع تحت-الليث ارينيت و أن

أكاسيد الحديد هى المادة اللاحمة الرئيسية والكوارتز يشغل معظم أرضية الصخر بينما يتميز الصخر الطفلى بوجود بعض الحبيبات الرملية داخل تركيبته الطينية مع تأثير واضح للمحاليل اللاحقة الغنية بأكاسيد الحديد والمنجنيز. أظهرت الدراسه الجيوكيميائية أن الحافة القارية النشطة والقوس الجزرى هما البيئات التكتونية التى تكون فيها صخرى الحجر الرملى والطفلة على التوالى. وقد سجلت تركيزات العناصر الأرضيه النادرة نسبه تتراوح من ٠,٤٩ إلى ٠,٨٣٪ فى الحجر الرملى فى حين أنها تراوحت من ٢٨٨ إلى ٥٢٦ جزء من المليون فى صخر الطفلة مع وجود بعض الدلالات على أن المعادن الإضافيه كانت العامل الأساسى المُتحكم فى تركيز و توزيع هذه العناصر في الصخور محل الدراسة و خاصةً الحجر الرملى.

هذا و قد خَلصت الدراسة إلى ضرورة الإهتمام بصخر الحجر الرملى بمنطقة أم جريفات كمصدر واعد لاستخلاص العناصر الأرضية النادرة وكذلك الحجر الطفلى كمصدر لإستخراج الزنك وذلك لاحتوائه على نسب عاليه من عنصر الزنك بمتوسط ٠,٨٦٪.